

Tuning the Morphology of Isoindigo Donor–Acceptor Polymer Film for High Sensitivity Ammonia Sensor

Chun-Fu Lu, Cheng-Wei Shih, Chien-An Chen, Albert Chin, and Wei-Fang Su*

Monitoring the ammonia gas is of great interest to both environmental benefits and human health. The recent advance in polymer thin film transistors (TFTs) can realize high sensitivity and low-cost gas sensors. Ammonia gas interacts with charge carrier channels and polymer/dielectrics interface through Coulomb force. This is the first report of high sensitivity and reusable ammonia sensor fabricated from thiophene-isoindigo donor–acceptor conducting polymer. This kind of polymer has advantages of simple synthesis and excellent air stability. The systematic study is carried out to investigate relationship among chemical structure variation and morphology control of polymer to the performance of ammonia sensor. High crystallinity, favored crystal orientation, and direct percolation routes for analytes are found to be essential to increase the susceptibility of polymers to ammonia gas. By strengthening edge-on morphology, the sensitivity can be enhanced fivefold for the same polymer. The idea can put forward the development of sensor array in a time-efficient manner by employing the morphology effect.

cause for airborne particulate matter.^[2] Gaseous ammonia in the atmosphere is generally produced from agricultural activities, manufacturing plants, vehicular emissions and volatilization from soils and oceans.^[3] Also, it is essential to monitor the concentration level of ammonia in breath for health since ammonia is recognized as a pathogenetic factor for Alzheimer's disease.^[4] Thus, a variety of ammonia sensors based on organic materials have been developed. Thin film transistors have multiparameters to achieve high sensitivity and discrimination between isomers, which is beyond the reach of chemiresistors alike. By improving the performance and stability of the device, the polymer TFTs have the potential to be mass produced and commercialized due to the polymer thin films can be solution processed with excellent film integrity, compared to small organic

1. Introduction

Polymer thin film transistors (TFTs) have been recently explored in sensor applications due to the continuous progress in materials and understanding of the polymer devices.^[1] The semiconducting polymers held several advantages in their easily tunable chemical structures and morphologies over their inorganic counterparts to achieve high sensitivity and good selectivity. One of the widely studied analytes is ammonia gas, a major volatile compounds in the atmosphere and one of the

molecule semiconductors with poor mechanical stability.

Ammonia generally interacts with the semiconducting polymers by either chemical reactions through specific functional groups^[5] or physical adsorption near the charge carriers.^[6] Zhang and co-workers^[7] have reported the improvement in sensitivity of the ammonia sensor by synthesizing designed functional groups in the polymer chemical structure. Although the direct interaction with the analytes is favored in many aspects, the diversity induced by the slight alteration of polymer structures has to be understood to clarify the influence besides chemical bonding. Without the aid of chemical reactions, ammonia usually influence the charge transport in two ways: (1) adsorbing on the polymers through Coulomb interaction,^[8] which reduces the conductance in p-type polymers; (2) accumulating at the polymer/ dielectrics interface,^[9] which changes the charge distribution at the interface and leads to threshold voltage (V_T) shifts. Typical approaches toward improving sensitivity of ammonia sensors involve increasing the surface area of the polymers^[9b] or exposing the carrier channels to analytes.^[10] However, polymer packing order and the morphology of polymer thin films are crucial to achieve high mobility. It is imperative to understand the morphology effect on both TFTs and gas sensors. The chemical structure of the polymers and the processing conditions can lead to different film morphology and shed light on how to tune the morphology with minimum sacrifice in charge transport capability.

Donor(D)–acceptor(A) copolymers possess the advantage of various chemical structures in the polymer main chain and superior TFT performance, comparing to homopolymers like

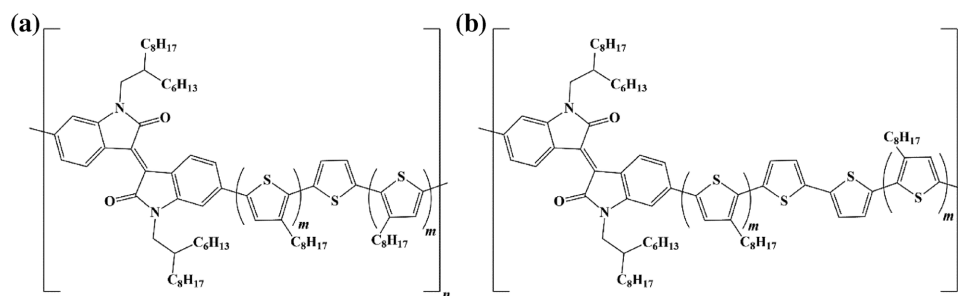
C.-F. Lu, Prof. W.-F. Su
Department of Materials Science and Engineering
Advanced Research Center for Green Materials Science and Technology
National Taiwan University
No. 1, Sec. 4, Roosevelt Road, Taipei City 10617, Taiwan
E-mail: suwf@ntu.edu.tw

C.-W. Shih, Prof. A. Chin
Department of Electronics Engineering
National Chiao Tung University
Hsinchu 300, Taiwan

C.-A. Chen, Prof. W.-F. Su
Institute of Polymer Science and Engineering
National Taiwan University
No. 1, Sec. 4, Roosevelt Road, Taipei City 10617, Taiwan

 The ORCID identification number(s) for the author(s) of this article can be found under <https://doi.org/10.1002/adfm.201803145>.

DOI: 10.1002/adfm.201803145



Scheme 1. Chemical structures of a) P3TI ($m = 1$) and P5TI ($m = 2$) and b) P4TI ($m = 1$) and P6TI ($m = 2$).

P3HT. Recently, a variety of air stable and high mobility D–A polymer TFT devices have been reported.^[1a,11] Good air stability is particularly important for gas sensors to achieve reliable sensing response and low detection limit. However, some of the D–A copolymers, such as diketopyrrolopyrrole-based polymers, require rigorous and complicated multisteps synthesis, which prolongs the sensor developing cycle. Considering the synthesis of polymers, D–A copolymers based on isoindigo are particularly attractive due to two reasons. (1) Isoindigo is a natural dye which can be extracted from plants. (2) It takes only two synthesis steps to prepare isoindigo polymers. Thus, isoindigo polymers are beneficial and environmental friendly for mass production in the future. Several groups have reported good sensing ability for metal ions detection in aqueous solution^[12] and discrimination of gaseous xylene isomers^[13] by utilizing isoindigo-based polymer TFTs. As far as we know, there are no reference using isoindigo-based polymer transistors as ammonia sensor. In addition, the morphology and electrical properties of D–A copolymers are also related to the chemical structures.^[14] It is particularly interesting to note that the slight changes in the donor segment can lead to different crystallinity and packing orientation of isoindigo-based polymers.^[15] With carefully designed chemical structures, we can explore the morphology effect to enhance sensitivity of ammonia sensors.

Herein, we aim for a simple solution to fabricate high sensitivity ammonia sensor: easy-to-synthesize polymers and simple device structure. We fabricated the devices by using a series of isoindigo-based D–A copolymers.^[16] The copolymers, P3TI, P4TI, P5TI, and P6TI, were consisted of different numbers of thiophenes in the donor segment and named accordingly. The different chemical structure among these $PnTI$ polymers can manifest in TFT characteristics, polymer packing, surface morphology, and sensitivity toward ammonia gas. We explored the morphology effect on polymer transistors and sensing capability thereof from the aspects of the chemical structure and the packing orientation of the polymers. In our polymer system, we found out that the susceptibility of polymer films to analytes depends heavily on both the polymer crystals quality and surface morphology. By exploring the morphology effect, reliable and real-time ammonia detection was realized at the concentration as low as 1 ppm in air. The

TFT sensors exhibit good air stability and long term stability—less than 10% decrease in mobility after storing 60 days in ambient condition. We also demonstrated significant sensibility difference from P6TI TFT devices by manipulating the polymer packing orientation through processing. The results provide a simple and efficient route for the development of high sensitivity and low cost sensor arrays.

2. Results and Discussion

2.1. Electrical Characteristics of $PnTI$ Transistors

The chemical structures of $PnTI$ polymers are shown in **Scheme 1** and the synthetic routes to each polymer are according to our previous work.^[16] The polymers used in this study have number-average molecular weight (M_n) and molecular weight distribution (PDI) in the range of 26–48k and 1.77–2.41, respectively. The TFT devices with the bottom-gate top-contact geometry are adopted to evaluate the field effect of the $PnTI$ polymers and served as ammonia sensors. Polymer thin films or devices are denoted as PnTI-CF or PnTI-DCB according to the processing solvent, chloroform (CF), or dichlorobenzene (DCB), respectively. In **Figure 1a**, the transfer curve of P3TI-CF transistor shows the typical I – V response of p-type materials and the hole mobility extracted from the saturation region is about $0.026 \text{ cm}^2 \text{ V}^{-1} \text{ s}^{-1}$. The device exhibits ignorable hysteresis and

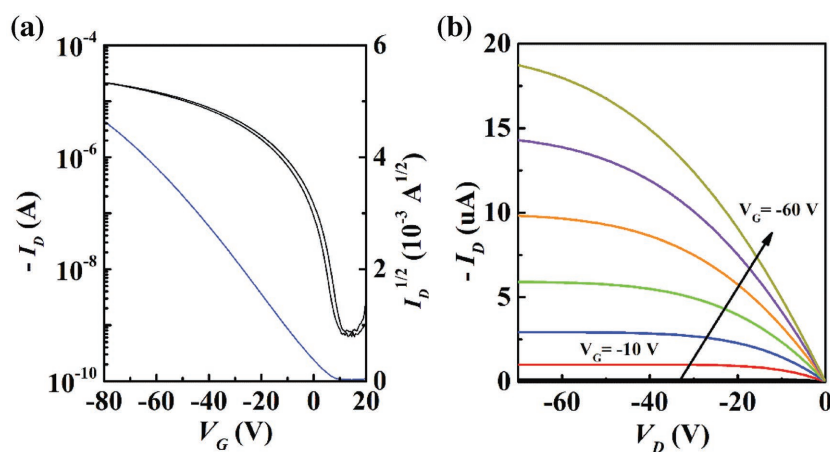


Figure 1. a) Transfer and b) out-put characteristics of a P3TI-CF transistor at $V_{DS} = -20 \text{ V}$ after annealing at 180°C under vacuum.

Table 1. Saturation mobility (μ_{sat}), on/off ratio, and threshold voltage (V_T) of *PnTI* transistors.

Sample	μ_{sat} [$\text{cm}^2 \text{V}^{-1} \text{s}^{-1}$]	On/off	V_T [V]
P3TI-CF	0.026 ± 0.001	$>10^4$	4.6 ± 0.6
P3TI-DCB	0.059 ± 0.007	$>10^5$	0.1 ± 2.1
P4TI-CF	0.017 ± 0.001	$>10^5$	-3.7 ± 3.4
P4TI-DCB	0.011 ± 0.002	$>10^4$	-0.1 ± 0.8
P5TI-CF	0.037 ± 0.001	$>10^4$	-3.0 ± 2.2
P5TI-DCB	0.053 ± 0.011	$>10^5$	2.5 ± 0.6
P6TI-CF	0.016 ± 0.002	$>10^4$	6.9 ± 1.0
P6TI-DCB	0.025 ± 0.002	$>10^5$	-2.0 ± 3.8

small contact resistance as indicated in the output characteristics in Figure 1b. The *PnTI* thin films fabricated from CF and DCB are investigated and the detailed TFT results are summarized in Table 1. Generally, the *PnTI* polymers have hole mobility around $0.1\text{--}0.01 \text{ cm}^2 \text{V}^{-1} \text{s}^{-1}$ with on/off ratio greater than 10^4 . The response of all *PnTI* TFTs are the same in both ambient and nitrogen environment. The results of long term stability are included in the Supporting Information. After storing in air for two months, the mobility of *PnTI* TFTs decays less than 10% from the average mobility in the first 5 days, indicating good air stability of the devices. For convenience, nitrogen served as a carrier for ammonia gas to evaluate the influence of ammonia and dry air was used in the real-time ammonia detection.

2.2. Thin Film Morphology of *PnTI* Films

In conventional gas sensors, increasing surface area is usually a robust way to induce high sensitivity and fast response. Several

groups^[9b,10] have reported high-performance gas sensors based on polymer transistors by exploring different morphology which corresponds to different surface area. For a TFT device, the shift in threshold voltage can produce an enormous difference in the source–drain current under the same operating gate voltage. Ammonia molecules can cause such difference by changing the charge distribution at the interface of semiconductor and dielectrics once they are adjacent to the dielectrics. Thus, to achieve high sensitivity ammonia sensor, the polymer films have to contain direct and unhindered percolation routes for ammonia gas to reach the polymer/dielectrics interface. To achieve this, large surface area and high crystallinity of polymer films are required. The polymer with highly ordered structures is beneficial for distinct and high crystallinity grains surrounding by grain boundaries.

Grazing incidence wide angle X-ray scattering (GIWAXS) was used to study the polymer morphology and crystallinity. The 2D GIWAXS images of *PnTI*-CF thin films in Figure 2 reveal the influence of the chemical structure of *PnTI* polymers on the polymer packing orientation and crystallinity. The calculated crystallographic parameters of the *PnTI* polymers are summarized in Table 2. In Figure 2a, P3TI-CF film has reflections from the lamellae structure in both out-of-plane (Q_z) and in-plane (Q_{xy}) directions, indicating P3TI packing along the substrate (edge-on) and perpendicular to the substrate (face-on), respectively. Thus, the P3TI-CF exhibits bimodal morphology having the edge-on and face-on lamellae crystals about equal intensity of crystallinity. The lamellar spacing (d_{100}) is 21.3 \AA , calculated from the (200) reflection in the out-of-plane line-cuts of the GIWAXS image. The signal at $Q_z = 1.64 \text{ \AA}^{-1}$ represents the π – π interaction of face-on crystals in the P3TI-CF film which has a π – π spacing of 3.7 \AA . In Figure 2b, the P5TI-CF film shows only clear (100) reflection in Q_z direction without any face-on signals. The lamellae spacing of P5TI-CF is determined

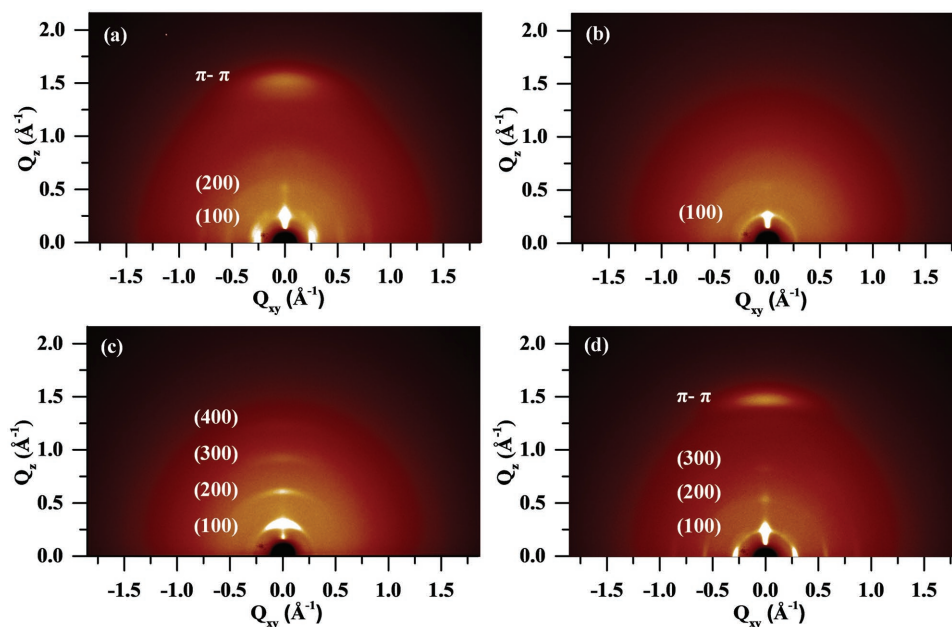


Figure 2. 2D grazing incidence wide angle X-ray scattering (GIWAXS) images of a) P3TI-CF, b) P5TI-CF, c) P4TI-CF, and d) P6TI-CF thin films. All films were annealed at the optimal temperature in vacuum for an hour.

Table 2. Crystallographic parameters, the lamellae spacing (d_{100}) and the coherence length (L_c) of $PnTI$ calculated from 2D GIWAXS.

Sample	d_{100} [Å]	L_c [Å]
P3TI-CF	21.3	71
P3TI-DCB	21.3	157
P4TI-CF	18.1	153
P4TI-DCB	18.2	143
P5TI-CF	20.6	353
P5TI-DCB	20.2	216
P6TI-CF	18.9	216
P6TI-DCB	18.6	153

as 20.6 Å, slightly smaller than that of P3TI-CF. From the chemical structure point of view, odd number of thiophenes in donor segment results in asymmetric polymer structures. The crystal structures are not very well-defined because the large spacing of alkyl side chains and twisted isoindigo segment are present in the P5TI-CF. The low order reflections are observed in the P3TI-CF as well as the P5TI-CF, and thus both thin films are of low crystallinity.

For the other two polymers, P4TI and P6TI are structurally symmetric with the even number of thiophenes in the repeating unit. The polymer films are expected to be orderly packed and crystalline. Similar odd–even effect in isoindigo-based D–A polymers were also reported by Pei and co-workers.^[15] As shown in Figure 2c, the P4TI-CF exhibits the reflection from the lamellae structure up to (400) in Q_z direction, indicating well-ordered edge-on morphology. The crystals of P4TI-CF are tightly packed into the lamellae structure, which is supported by the small lamellae spacing of 18.1 Å. With the isoindigo segments connected by even number of thiophenes with minimum twists, the spacing between polymer chains is reduced and the planarity of P4TI is improved. The strong intermolecular interaction of P4TI allows the polymer to self-aggregate easily, leading to ordered crystalline structures in the thin film. The other symmetric polymer, P6TI-CF, also has good crystallinity. It is supported by the clear (300) reflection shown in Figure 2d, small d_{100} of 18.9 Å and small full width at half maximum of π – π interaction peak. The difference between P4TI-CF and P6TI-CF lies in the orientation of crystals. While P4TI-CF has uniformly edge-on crystals, P6TI-CF has bimodal morphology, in which lamellae structures are observed in both Q_z and Q_y directions. There are two reasons for face-on crystals to be present in P6TI-CF. First, P6TI contains two more alkyl side chains on thiophenes than that of P4TI in each repeating unit of respective polymer. The alkyl side chains take time to arrange themselves to the ordered structure. The more of the side chains are, the more time the process takes. The second reason is the use of low boiling point chloroform solvent (63 °C). It has little time for P6TI to form crystals because chloroform evaporates rather quickly. Thus, the P6TI-CF contains crystals with two orientations: aligned along and perpendicular to the substrate.

It is clear that asymmetric polymer structures leads to thin films with moderate crystallinity while symmetric polymer structures produce high crystallinity thin films. The evaporation rate of the processing solvent also affects the polymer packing

because the polymer chains take time to rearrange and pack into crystals. To provide more time for polymers to form ordered crystals, high boiling point solvent DCB is used to compare with CF. The GIWAXS images of $PnTI$ -DCB are shown in the Supporting Information. The GIWAXS study reveals two major influence of DCB on the formation of polymer crystals. First, the polymer films made from DCB result in higher crystallinity than those fabricated from CF. The P5TI-DCB and P6TI-DCB have smaller lamellae spacing (d_{100}) than P5TI-CF and P6TI-CF as summarized in Table 2. The small d_{100} indicates tightly packed polymer crystals. The clear difference in d_{100} from solvent effect for P5TI and P6TI is partly because there are more side chains on those two polymers and they take long time to be orderly packed. For P3TI-DCB and P4TI-DCB films, the lamellae spacing is the same with their CF-fabricated counterparts since there are only two alkyl side chains in the repeating unit of each polymer. Considering the polycrystalline nature of polymers, coherence length (L_c) was calculated to represent the crystalline domain size with the compensation of the cumulative disorder.^[17] The coherence length of P3TI-DCB is two times longer than P3TI-CF, indicating larger polymer crystals. The other impact of using DCB as processing solvent is the unidirectional polymer packing orientation. All $PnTI$ -DCB films show reflections from lamellae structures in only Q_z direction, indicating dominantly edge-on morphology regardless of the polymer chemical structure. Therefore, we can tune the morphology of the P3TI and P6TI thin films from bimodal to edge-on by using different solvents during processing.

2.3. Surface Morphology of $PnTI$ Films

Efficient diffusion route for ammonia gas in the polymer film is another important factor to achieve high sensitivity sensor. In the TFT devices, charge carriers mainly transfer near the dielectrics due to the strong electric field. Ammonia molecules have to reach the dielectrics/polymer interface or charge carrier channels to change the polymer transistor characteristics. Continuous and direct pathways are favored for fast detection of analytes, provided that such pathways do not affect carrier transport in the polymer thin films. Surface morphology of $PnTI$ films is probed by tapping mode atomic force microscopy (AFM). All $PnTI$ films have smooth surface without micrometer-sized structures or aggregates, as indicated by the low average surface roughness of 0.585, 0.592, 0.802, and 0.460 nm for P3TI-CF, P4TI-CF, P5TI-CF, and P6TI-CF, respectively. Figure 3a shows the surface morphology of P3TI-CF and the height curve using the line section. The surface of P3TI-CF is consisted of bundles of fibers about the size of 10 to 40 nm. The small fibrous structures are composed of polymer crystals and the surrounding amorphous polymer chains. The spacing between the polymer fibers is mostly discrete and small, which gives P3TI-CF inefficient diffusion pathways. In Figure 3b, the other asymmetric polymer film, P5TI-CF, appears to have spherical structures. The assembled structures are in the range of 30–80 nm. The spacing between the structures is larger in P5TI-CF than P3TI-CF but the percolation routes are winding which deter the direct diffusion path for analyte gas. By contrast, the P4TI-CF exhibits large plate-like and continuous structures in horizontal direction as shown in Figure 3c. Through the line section, we can observe three kinds

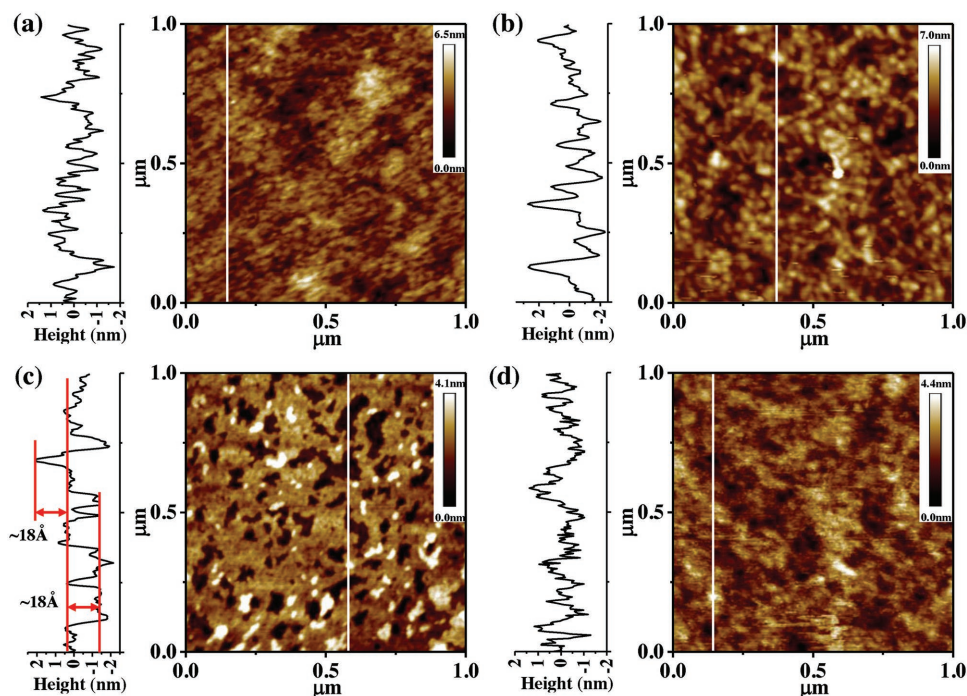


Figure 3. AFM images of a) P3TI-CF, b) P5TI-CF, c) P4TI-CF, and d) P6TI-CF thin films. The height profiles are the line sections marked by the white lines in the figures.

of structural morphology (from the top to the bottom of surface): (a) small white aggregate area, (b) yellowish brown area: a layer of P4TI polymer, and (c) dark brown area observed through the voids of yellowish brown area: another layer of polymer. The dark brown areas observed through the voids are part of another layer of polymer and the small white areas are on the top of the brown layer. The line section reveals that the height difference, between two layers of polymers or between the white spots and the brown layer, is about 18 Å, consistent with the d_{100} of P4TI-CF calculated from X-ray scattering study. Such large-scale ordered structure results from the high crystallinity and edge-on only packing orientation of P4TI. Ammonia can easily reach the bottom layer of polymers and dielectrics surface through the voids of the top layer of P4TI-CF. The favorable surface morphology accompanied with edge-on crystals may increase the sensitivity of P4TI-CF to ammonia gas. Figure 3d finds that the other symmetric polymer film, the P6TI-CF, does not have the layered structures as shown in the P4TI-CF. Instead, the P6TI-CF exhibits small fibrous structures. The sizes of the fibers are in the range of 8–20 nm. The symmetric chemical structure of P6TI leads to tightly packed crystals. However, containing both edge-on and face-on crystals, it is hard for the P6TI-CF to form large-scaled ordered structures. Thus, small fibers instead of layered structures are prevalent in the P6TI-CF. The diffusion pathways for ammonia are also hindered in the P6TI-CF.

2.4. Morphology Effect on the Sensitivity to Ammonia

To correlate the morphology effect and ammonia detection, the *PnTI* TFTs are first characterized under a set of ammonia environments (0, 1, 5, 10, 20, and 50 ppm). Figure 4a,b shows

the transfer curves of the P3TI-CF and the P4TI-CF with and without ammonia exposure. The P3TI-CF represents the film with low crystallinity and winding diffusion pathways while the P4TI-CF stands for the film with high crystallinity and direct percolation routes. The P3TI-CF retains most of its on-off characteristics: the drain current value, the on-off ratio, the mobility, and the threshold voltage. A small threshold voltage shift (ΔV_T) of 1.5 V manifests in the presence of 50 ppm ammonia. The small ΔV_T is because of the bimodal morphology and the discrete spacing in the film. On the other hand, the transfer curves of the P4TI-CF have large shifts toward negative with increasing ammonia concentration. The threshold voltage of the P4TI-CF shifts 4.1 V in merely 10 min exposure to 1 ppm ammonia and ΔV_T under 50 ppm ammonia is sixfold larger than that of the P3TI-CF. The dramatic changes in the characteristics of the P4TI-CF are due to the following two reasons. The first reason is the highly crystalline crystals packed in edge-on orientation. The amorphous polymers only take a small percentage in a high crystallinity polymer film. Ammonia molecules can physically absorb on the charge carriers channels easily. The unidirection of charge transport in edge-on packing polymer film also contributes to the cause. The second reason is the efficient diffusion pathways for ammonia to permeate through the polymer film and reach the dielectric surface. Layered structures and large voids are beneficial to accomplish this goal. The significant differences between the P3TI-CF and the P4TI-CF mainly arise from the well-ordered, edge-on only polymer packing and the direct percolation paths for ammonia gas in the P4TI-CF thin films. Thus, the P4TI-CF has higher sensitivity to ammonia than the P3TI-CF by having favored morphology, which even overcomes its inferior mobility of $0.017 \text{ cm}^2 \text{ V}^{-1} \text{ s}^{-1}$.

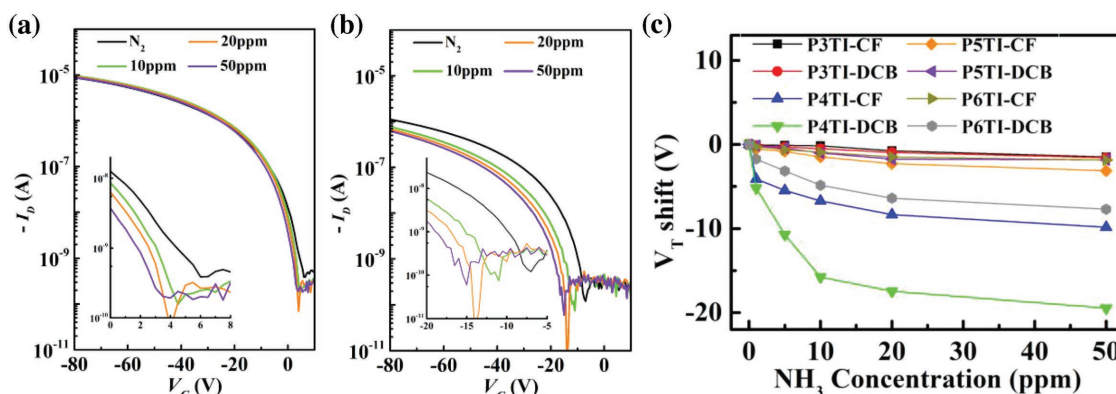


Figure 4. Transfer curves of a) P3TI-CF TFT and b) P4TI-CF TFT in nitrogen, 1, 5, 10, 20, and 50 ppm NH_3 . The insets show the enlarged transfer curves at the turn-on points. c) Threshold voltage shift (ΔV_T) of $PnTI$ TFTs when exposing to different concentration of ammonia vapor.

Figure 4c shows the threshold voltage changes of $PnTI$ -CF and $PnTI$ -DCB. All P3TI and P5TI devices exhibit little difference in V_T . This is due to the low crystallinity originated from their asymmetric chemical structures. Large amount amorphous polymers cover the crystals well (few voids) that slow down the permeation rate of ammonia from top of the device to the carrier channels and polymer/dielectrics interface. The charge distribution near the dielectric interface is not affected much by the influx of ammonia and there are merely slight changes in the charge carrier concentration of the polymer. Therefore, charge carrier transports in P3TI and P5TI TFTs retain most of their intrinsic characteristics regardless of using high boiling point solvent or not. For highly crystalline P4TI, the P4TI-DCB shows even larger ΔV_T than the P4TI-CF. The reason, however, is the effective and direct diffusion paths in the film rather than the crystallinity. As discussed in the previous sections, the P4TI-CF has high crystallinity, edge-on packing orientation, and favored surface morphology. The P4TI-DCB has the equal crystallinity and the same crystals orientation as determined by GIWAXS. The main difference lies in the surface morphology of the two films. The AFM image (Figure S4, Supporting Information) of P4TI-DCB shows several voids that can reach 55 Å (three layers of P4TI) below the top layer of polymer. These voids provide direct diffusion paths for ammonia to reach deep into the polymer film. Therefore, with more effective pathways to diffuse to the polymer/dielectric interface, P4TI-DCB exhibit higher sensitivity than P4TI-CF.

Highly crystalline polymer films do not always have high sensitivity. Despite of its high crystallinity, the P6TI-CF exhibits only small ΔV_T after exposing to ammonia. By contrast, the P6TI-DCB shifts five times larger in V_T than that of the P6TI-CF. The main difference lies in the tightness of crystal packing in the P6TI-CF and P6TI-DCB. To compare the difference between edge-on and bimodal thin films and their susceptibility to ammonia, the charge distribution changes by ammonia molecules at the dielectric interface in each film are illustrated in Figure 5. Here we consider the adjacent polymer layer to the dielectric because it directly decides the characteristics of the device. In the case of edge-on morphology, there are voids between crystals because not every crystals are strictly edge-on. Polymers do not cover all of dielectric surface due to these voids. The voids between polymer crystals can thus serve as the diffusion pathways for ammonia. Also, the spacing between crystal and dielectric is large due to the long alkyl side chains and octadecylsilane monolayer on top of the SiO_2 dielectric. Ammonia gas can diffuse into these spacing through the voids between the crystals. Then, ammonia molecules change the charge distribution at the polymer/dielectric interface, leading to large V_T shift. On the other hand, we speculate that the bimodal morphology keep the polymer/dielectric interface from the influence of ammonia gas. The alkyl side chains of face-on crystals are parallel to the substrate, which allow the face-on crystals to be closer to the dielectric

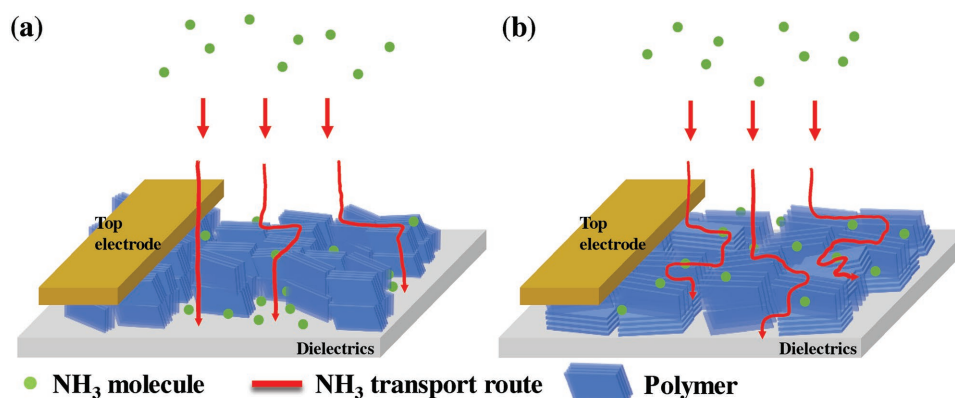


Figure 5. Schematic diagrams of intake and transport routes of ammonia molecules in a) edge-on morphology and b) bimodal morphology.

at the interface than edge-on crystals. With both edge-on and face-on crystals packed closely, bimodal polymer films have greater coverage near the dielectrics interface than edge-on polymer films. The voids near the dielectric are scarce. Thus, polymers with bimodal morphology can retain the threshold voltage by shielding the dielectrics from ammonia gas. Therein accounts for the different ΔV_T of P6TI-CF and P6TI-DCB when exposing to ammonia. The idea is particularly useful for building sensor arrays by tuning the morphology rather than synthesizing different polymers, which can be quite time-consuming.

2.5. In Situ Ammonia Detection

Real-time ammonia detecting is carried out by exposing the *PnTI* TFTs to different concentrations of ammonia in air. The P3TI-CF and P4TI-CF TFTs are used to demonstrate the sensitivity difference caused by packing symmetry and surface morphology. **Figure 6** shows that the P4TI-CF is more sensitive than the P3TI-CF. The sensing response was defined by the following equation

$$R = \frac{I_D(0) - I_D(t)}{I_D(0)} \quad (1)$$

where $I_D(t)$ and $I_D(0)$ are the drain current at time t and the start of the measurement, respectively. The response of P4TI-CF is easily twice as large as that of P3TI-CF since the threshold voltage of P4TI-CF shifts rather dramatically in the presence of ammonia. We are able to detect 1 ppm ammonia with P4TI-CF TFT directly. Edge-on morphology, high crystallinity, and large percolation paths for analytes are clearly beneficial to achieve fast response and highly sensitive ammonia sensor. The reusability of the TFT sensors is also investigated. The *PnTI* TFTs sensors can be reset by expelling the trapped ammonia molecules with a positive gate bias, which accelerate the desorption process. Direct diffusion pathways are also preferred in resetting the device.

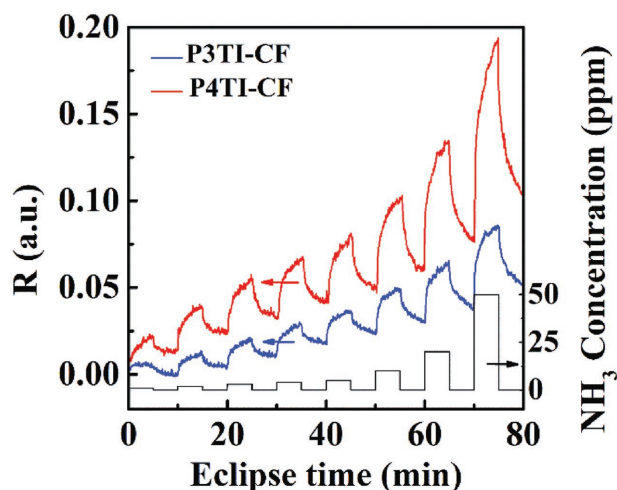


Figure 6. Sensor response of P3TI-CF and P4TI-CF to ammonia concentration from 1 to 50 ppm in air. (1, 2, 3, 4, 5, 10, 20, and 50 ppm) P3TI-CF and P4TI-CF are both operated at $V_{GS} = -30$ V and $V_{DS} = -30$ V.

2.6. Comparison with State-of-the-Art Ammonia Sensors Based on Polymer TFT

In real practice, ammonia sensors with different detection range are required for specific application. For instance, the leakage from chemical plants generally lies in the range of 20–1000 ppm^[18] while the household alarms require detection limit lower than 20 ppm, meeting the recommended exposure limit of 25 ppm established by the U.S. National Institute for Occupational Safety and Health.^[19] On the other hand, ultrasensitive ammonia sensors (detection range in 1 ppb to 1 ppm) are suitable for medical diagnosis of Alzheimer's disease or kidney disorder. Polymer transistors can realize full range detection of ammonia by improving air stability and reversibility. The *PnTI* TFT sensors possess these two important criteria. Numerous high-performance ammonia sensors based on polymers have been reported in the literature and they are summarized in **Table 3**. Among these reported highly sensitive sensors, two strategies are

Table 3. Comparison with recently reported ammonia sensors based on polymer TFTs.

Materials (functional group)	Film structure	Detection range [ppm]	Response time ^{a)}	Air stability ^{b)}	Reversibility ^{c)}	Ref.
P3HT	Plain	0.1–25	5–25 s	Y	N.A.	[8]
P3HT/PS	Structured	5–50	5–10 min	Y	Y	[20]
PBTBT	Nanostructured	10–100	5–15 s	Y	Y	[9b]
PBIBDF-BT	Porous	0.5–50	8 s ^{d)}	N.A.	Y	[21]
DPPT-TT	Nanostructured	10	1–3 min	Y	Y	[22]
P4TI	Plain	1–100	1–3 min	Y	Y	This work
PTTEH (C=O)	Plain	0.01–100	20–40 s ^{e)}	N.A.	Y	[23]
pDPPCOOH-BT (COOH)	Nanoporous	0.01–1000	5–10 s	Y	Vacuum	[7]
PDFDT (F)	Plain	1–1000	1–2 min	Y	Y	[9a]
DPP2T-TT/PVP-HDA (OH, COOH, F)	Nanoporous	0.001–100	1–10 s	Y	Y	[10]

^{a)}Response time is estimated from the time-dependent response curves at the 80% of the maximum response value if the data are not available in the reference; ^{b)}The air stability is determined by whether air is the carrier gas used in the experiment or not; ^{c)}Reversibility is determined by whether there are multiple measurements in the time-dependent response curves or other supporting data; ^{d)}The value is based on the measurement under 10 ppm NH₃; ^{e)}The value is based on the measurement under 100 ppm NH₃.

generally adopted to achieve high sensitivity and fast response: increasing surface area of polymers and incorporating functional groups such as carboxylic acid or fluorine. However, these methods require extra care and efforts in preparation. Increasing surface area usually involves complex processing, which leads to large batch-to-batch variation. For incorporating functional groups in polymers, multistep synthesis indicates long development time and is challenging for scale-up in the future. In contrast, with simple processing and synthesis, the *PnTI* TFT sensors exhibit comparable sensitivity with the best reported ammonia sensors. The promising results of this research confirm that the strategy of tuning the morphology of conducting polymers to have edge-on morphology, high crystallinity, and large percolation paths for analytes can indeed improve the sensitivity and response time of the sensor. This idea can further the development of new polymer transistor-based sensors.

3. Conclusion

In this work, we have investigated the impact of the chemical structures and the thin film morphology of the *PnTI* polymers on the susceptibility to ammonia and tuning the favorable morphology toward high sensitivity. GIWAXS study in conjunction with surface morphology analysis elucidated the observed changes upon intake of ammonia gas. High sensitivity and fast response ammonia sensors can be achieved by exploring the trapping effect at the interfaces of polymer crystals/crystals and polymer crystals/dielectrics. Polymer films consisted with high crystallinity and ordered crystals in only edge-on direction tend to have favored morphology. The efficient diffusion pathways in the film allow ammonia to change the charge distribution in the device and result in large threshold voltage shifts after exposing to ammonia. On the other hand, polymers with low crystallinity or bimodal morphology show slow and small response to analytes. The degree of winding of percolation routes is different in each case and the charge transport routes are not readily affected by ammonia. We demonstrated the morphology of P6TI can be easily tuned by processing methods to achieve favored edge-on packing from bimodal packing. Through tuning the morphology of polymer thin films, it would be time-efficient to build sensor arrays to discriminate mixed analytes.

4. Experimental Section

Materials: The synthesis method of *PnTI* polymers was according to the previous work^[16] with modification at the microwave power and reaction time to obtain high molecular weight. The number-average molecular weight (M_n) and molecular weight distribution (PDI) were in the range of 26–48k and 1.77–2.41, respectively. Both values were determined by high temperature gel permeation chromatography at 135 °C, using 1,2,4-trichlorobenzene as eluent and monodisperse polystyrene as the calibration standard. All chemical reagents were purchased from Sigma-Aldrich or Acros and used as received unless otherwise mentioned.

Device Fabrication: The polymers were fabricated into thin film transistors with the bottom-gate top-contact geometry. The *PnTI* polymers were spin-cast from either chloroform (0.27 wt%) or *o*-dichlorobenzene (0.50 wt%) solution onto OTS-modified 300 nm SiO_2/n^{++} Si substrates. Polymer thin films or devices were denoted as PnTI-CF or PnTI-DCB

according to the processing solvent. P5TI thin films were subsequently annealed at 210 °C in vacuum for an hour while the annealing process for other polymers was performed at 180 °C to have optimal performance. The polymer films were cooled slowly to room temperature. Au source/drain electrodes of 100 nm thick were then thermally evaporated on top of polymer films through shadow masks. The channel length (L) and the channel width (W) were 100 μm and 1 mm, respectively.

Measurement: Electrical properties of the *PnTI* TFTs were measured by using a precision source/measurement unit (Keysight, B2912A) in addition to the probe station or the temperature controlled stage (Linkam Scientific, UK). The mobility (μ) was extracted from the saturation region and calculated by the formula

$$\mu_{\text{sat}} = \frac{\left(\frac{d\sqrt{I_{\text{SD}}}}{dV_{\text{SG}}}\right)^2}{\frac{1}{2}C_i \frac{W}{L}} \quad (2)$$

where I_{SD} is the source–drain current, V_{SG} is the source–gate voltage, W and L are the channel width and length, and C_i is the dielectric constant of SiO_2 (10^{-4} F m^{-2}). The measurements of GIWAXS of the thin films were performed at National Synchrotron Radiation Research Center in Taiwan, using beamline 17A. The samples were prepared as described above. The incident angle of X-ray was carefully adjusted to 0.2° by aligning the thin film for each measurement. The surface morphology of polymer thin films was examined by tapping mode of atomic force microscopy (OMV-NTSC, Bruker). For ammonia sensors, the TFTs were measured in the temperature controlled stage, which was equipped with air-tight sealing. The ammonia environments were first prepared by using mass flow controllers (Alicat, US) and then transported into the temperature controlled stage. In most of the sensor measurements, nitrogen served as the carrier gas and various concentrations of ammonia were diluted from 1000 ppm NH_3 in N_2 . For the in situ sensor response measured in air, the carrier gas was dry air and the ammonia environment was prepared from 50 ppm NH_3 in air. The sensors were measured at 20 °C and 1 atm.

Supporting Information

Supporting Information is available from the Wiley Online Library or from the author.

Acknowledgements

This work was financially supported by the “Advanced Research Center for Green Materials Science and Technology” from The Featured Area Research Center Program within the framework of the Higher Education Sprout Project by the Ministry of Education (107L9006) and the Ministry of Science and Technology in Taiwan (MOST106-2218-E-002-021-MY2 and 107-3017-F-002-001). The authors also thank the partial financial support from the grant of MOST106-2923-M-002 -004 -MY3.

Conflict of Interest

The authors declare no conflict of interest.

Keywords

ammonia sensors, field-effect transistors, morphology, packing orientation, polymers

Received: May 7, 2018

Revised: July 13, 2018

Published online: August 14, 2018

- [1] a) H. N. Tsao, D. M. Cho, I. Park, M. R. Hansen, A. Mavrinskiy, D. Y. Yoon, R. Graf, W. Pisula, H. W. Spiess, K. Mullen, *J. Am. Chem. Soc.* **2011**, *133*, 2605; b) F. Zhang, C. A. Di, N. Berdunov, Y. Hu, Y. Hu, X. Gao, Q. Meng, H. Siringhaus, D. Zhu, *Adv. Mater.* **2013**, *25*, 1401; c) R. Noriega, J. Rivnay, K. Vandewal, F. P. Koch, N. Stingelin, P. Smith, M. F. Toney, A. Salleo, *Nat. Mater.* **2013**, *12*, 1038.
- [2] S. N. Behera, R. Betha, P. Liu, R. Balasubramanian, *Sci. Total Environ.* **2013**, *452–453*, 286.
- [3] S. N. Behera, M. Sharma, V. P. Aneja, R. Balasubramanian, *Environ. Sci. Pollut. Res. Int.* **2013**, *20*, 8092.
- [4] N. Seiler, *Neurochem. Int.* **2002**, *41*, 189.
- [5] Y. Gannot, C. Hertzog-Ronen, N. Tessler, Y. Eichen, *Adv. Funct. Mater.* **2010**, *20*, 105.
- [6] A. Lv, Y. Pan, L. Chi, *Sensors* **2017**, *17*, 213.
- [7] Y. Yang, G. Zhang, H. Luo, J. Yao, Z. Liu, D. Zhang, *ACS Appl. Mater. Interfaces* **2016**, *8*, 3635.
- [8] S. Tiwari, A. K. Singh, L. Joshi, P. Chakrabarti, W. Takashima, K. Kaneto, R. Prakash, *Sens. Actuators, B* **2012**, *171–172*, 962.
- [9] a) B. Nketia-Yawson, A. R. Jung, Y. Noh, G. S. Ryu, G. D. Tabi, K. K. Lee, B. Kim, Y. Y. Noh, *ACS Appl. Mater. Interfaces* **2017**, *9*, 7322; b) S. H. Yu, J. Cho, K. M. Sim, J. U. Ha, D. S. Chung, *ACS Appl. Mater. Interfaces* **2016**, *8*, 6570.
- [10] F. Zhang, G. Qu, E. Mohammadi, J. Mei, Y. Diao, *Adv. Funct. Mater.* **2017**, *27*, 1701117.
- [11] a) T. Lei, Y. Cao, Y. Fan, C. J. Liu, S. C. Yuan, J. Pei, *J. Am. Chem. Soc.* **2011**, *133*, 6099; b) Y. Gao, Y. Deng, H. Tian, J. Zhang, D. Yan, Y. Geng, F. Wang, *Adv. Mater.* **2017**, *29*, 1606217; c) G. Kim, S. J. Kang, G. K. Dutta, Y. K. Han, T. J. Shin, Y. Y. Noh, C. Yang, *J. Am. Chem. Soc.* **2014**, *136*, 9477; d) H.-W. Lin, W.-Y. Lee, W.-C. Chen, *J. Mater. Chem.* **2012**, *22*, 2120.
- [12] O. Knopfmacher, M. L. Hammock, A. L. Appleton, G. Schwartz, J. Mei, T. Lei, J. Pei, Z. Bao, *Nat. Commun.* **2014**, *5*, 2954.
- [13] B. Wang, T. P. Huynh, W. Wu, N. Hayek, T. T. Do, J. C. Cancilla, J. S. Torrecilla, M. M. Nahid, J. M. Colwell, O. M. Gazit, S. R. Puniredd, C. R. McNeill, P. Sonar, H. Haick, *Adv. Mater.* **2016**, *28*, 4012.
- [14] a) R. Stalder, S. R. Puniredd, M. R. Hansen, U. Koldemir, C. Grand, W. Zajaczkowski, K. Müllen, W. Pisula, J. R. Reynolds, *Chem. Mater.* **2016**, *28*, 1286; b) W.-T. Park, G. Kim, C. Yang, C. Liu, Y.-Y. Noh, *Adv. Funct. Mater.* **2016**, *26*, 4695.
- [15] T. Lei, J. Y. Wang, J. Pei, *Acc. Chem. Res.* **2014**, *47*, 1117.
- [16] C.-C. Ho, C.-A. Chen, C.-Y. Chang, S. B. Darling, W.-F. Su, *J. Mater. Chem. A* **2014**, *2*, 8026.
- [17] J. Rivnay, S. C. Mannsfeld, C. E. Miller, A. Salleo, M. F. Toney, *Chem. Rev.* **2012**, *112*, 5488.
- [18] B. Timmer, W. Olthuis, A. v. d. Berg, *Sens. Actuators, B* **2005**, *107*, 666.
- [19] *The National Institute for Occupational Safety and Health*, International Chemical Safety Cards, <https://www.cdc.gov/niosh/ipcsneng/neng0414.html> (accessed: July 2018).
- [20] S. Han, X. Zhuang, W. Shi, X. Yang, L. Li, J. Yu, *Sens. Actuators, B* **2016**, *225*, 10.
- [21] Q. Wang, S. Wu, F. Ge, G. Zhang, H. Lu, L. Qiu, *Adv. Mater. Interfaces* **2016**, *3*, 1600518.
- [22] D. Khim, G. S. Ryu, W. T. Park, H. Kim, M. Lee, Y. Y. Noh, *Adv. Mater.* **2016**, *28*, 2752.
- [23] Z. Wang, Z. Liu, L. Chen, Y. Yang, J. Ma, X. Zhang, Y. Guo, G. Zhang, D. Zhang, *Adv. Electron. Mater.* **2018**, *4*, 1800025.